Experimental and DFT-D studies of the molecular organic energetic material RDX

Cite as:
Morrison, C., Sutinen, T., Parker, S. F., Williamson, D. M., Thompson, S., Gould, P. J., Pulham, C., & Hunter, S. (2013). Experimental and DFT-D studies of the molecular organic energetic material RDX. *Journal of Physical Chemistry C*, 117(16), 80628-71.

Manuscript received: 15/01/2013; Accepted: 27/03/2013; Article published: 12/04/2013

Experimental and DFT-D Studies of the Molecular Organic Energetic Material RDX**

Steven Hunter,[1] Tuuli Sutinen,[2] Stewart F. Parker,[3] Carole A. Morrison,[1,*] David M. Williamson,[2] Stephen Thompson,[4] Peter J. Gould[5] and Colin R. Pulham[1,*]

[1]EaStCHEM, School of Chemistry and Centre for Science at Extreme Conditions, Joseph Black Building, University of Edinburgh, West Mains Road, Edinburgh, EH9 3JJ, UK.

[2]Department of Physics, University of Cambridge, Cavendish Laboratory, J J Thomson Avenue, Cambridge, CB3 0HE, England, UK.

[3]ISIS Neutron and Muon Facility, Rutherford Appleton Laboratory, Harwell Science and Innovation Campus, Didcot, Oxfordshire, OX11 0QX, England, UK.

[4]Diamond Light Source, Rutherford Appleton Laboratory, Harwell Science and Innovation Campus, Didcot, Oxfordshire, OX11 0QX, England, UK.

[5]QinetiQ Bristol, Building 240, The Close, Bristol Business Park, Coldharbour Lane, Bristol, BS16 1FJ, England, UK.

[*]Corresponding author; C.A.M e-mail: carole.morrison@ed.ac.uk; C.R.P e-mail: c.r.pulham@ed.ac.uk

[**]We gratefully acknowledge Dr. Philip J. Camp (The University of Edinburgh) for helpful discussions. We thank the Scottish Funding Council (SPIRIT) and QinetiQ (in support of MOD research) for contribution toward a studentship (S.H.); the ESPRC for the provision of high-performance computing time and The Department of Materials Science, University of Cambridge, for use of the DSC module. This work made use of the facilities of HECToR, the UK's national high-performance computing service, which is provided by UoE HPCx Ltd at the University of Edinburgh, Cray Inc. and NAG Ltd., and funded by the Office of Science and Technology through

EPSRC's High End Computing Programme. We acknowledge the support of the Diamond Light Source, STFC, and the ISIS Neutron and Muon Facility.

Supporting information:
The remaining DSC thermograms for β-RDX (Figures S1−S4); a comparison between the calculated lattice parameters and unit cell volumes for α- and γ-RDX, compared to previous DFT-D studies as well as relevant experimental data (Figures S5 and S6); comparison of predicted INS spectra for α-RDX to those for γ- and ε-RDX at similar pressures (Figures S7 and S8); a comparison of the DFT-D predicted crystallographic parameters with corresponding experimental data for α-, γ-, and ε-RDX (Tables S1, S3, and S4, respectively); full lists of calculated phonon modes as a function of pressure for α-, γ-, and ε-RDX compared to experimental Raman data, including pressure-induced shift values (Tables S2, S5, and S6). This material is available free of charge via the Internet at http://pubs.acs.org

Graphical abstract:

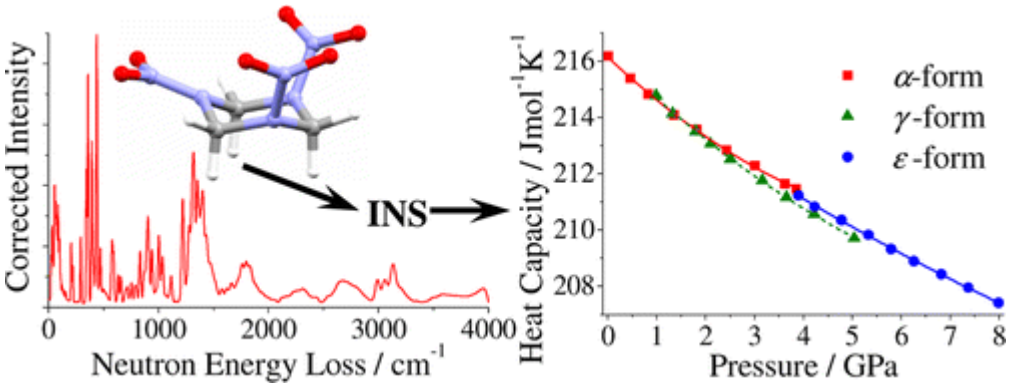

Abstract:
We have performed simulations utilizing the dispersion-corrected density functional theory method (DFT-D) as parametrized by Grimme on selected polymorphs of RDX (cyclotrimethylenetrinitramine). Additionally, we present the first experimental determination of the enthalpy of fusion (ΔH_{fus}) of the highly metastable β-form of RDX. The characteristics of fusion for β-RDX were determined to be 186.7 ± 0.8 °C, 188.5 ± 0.4 °C, and 12.63 ± 0.28 kJ mol^{-1} for the onset temperature, peak temperature (or melting point), and ΔH_{fus}, respectively. The difference in experimental ΔH_{fus} for the α- and β-forms of RDX is 20.46 ± 0.92 kJ mol^{-1}. Ambient-pressure lattice energies (E_L) of the α- and β-forms of RDX have been calculated and are in excellent agreement with experiment. In addition the computationally predicted difference in E_L (20.35 kJ mol^{-1}) between the α- and β-forms is in excellent agreement with the experimental difference in ΔH_{fus}. The response of the lattice parameters and unit-cell volumes to pressure for the α- and γ-forms have been investigated, in addition to the first high-pressure computational study of the ε-form of RDX—these results are in very good agreement with experimental data. Phonon calculations provide good agreement for vibrational frequencies obtained from Raman spectroscopy, and a predicted inelastic neutron scattering (INS) spectrum of α-RDX shows excellent agreement with experimental INS data determined in this study. The transition energies and intensities are reproduced, confirming that both the eigenvalues and the eigenvectors of the vibrations are correctly described by the DFT-D method. The results of the high-pressure phonon calculations have been used to show that the heat capacities of the α-, γ-, and ε-forms of RDX are only weakly affected by pressure.

1. Introduction

In the field of energetic materials (explosives and propellants), research is focused on the development of insensitive munitions that improve safety by reducing the risk of accidental initiation. The ambition is to design tailored energetic materials that have both specific functionality and a high threshold for accidental combustion or detonation. Due to the nature of the operational conditions (high temperatures and pressures) experienced by these materials, it is important to know not only the physical properties of the components at ambient temperatures and pressures, but also to understand how the structure and properties are affected by extreme conditions. Of particular importance is the development of an understanding of the factors that affect the deflagration-to-detonation transition (DDT) of high explosives (HE), *i.e.* the point at which a subsonic deflagrating reaction becomes a supersonic detonation. Since the rate of a deflagrating reaction depends upon temperature, it is necessary to know how the liberated thermal energy is partitioned within the energetic material to increase its temperature. Moreover, when a material deflagrates it will also experience an elevation in pressure. Thus, in order to understand the deflagration-to-detonation process better, it is important to understand how the specific heat capacity of the energetic material changes with respect to both temperature and pressure.

Pressure can also induce phase transitions in energetic materials resulting in different crystal structures (polymorphs) with different physical properties. In this study we have used a combination of experimental and computational methods to investigate the structure and selected properties of different polymorphs of the widely used explosive, RDX (cyclotrimethylenetrinitramine, see **Figure 1** for molecular structure), under ambient pressure and high-pressure conditions.

RDX is a secondary high explosive commonly used in military applications. At ambient temperature and pressure, the thermodynamically stable phase is the α-form, the crystal structure of which has been determined by both single crystal X-ray[1] and neutron diffraction studies.[2] The ambient pressure vibrational properties of α-RDX have been extensively studied by polarized Raman spectroscopy,[3,4,5] and more recently by inelastic neutron scattering (INS).[6] At ambient pressure there also exists a metastable β-form of RDX, which was first identified in 1950 by McCrone[7] and has subsequently been studied using vibrational spectroscopy.[8,9] On account of its high metastability with respect to the α-form, it was only recently structurally characterized.[10] There has been a long-standing assumption that β-RDX could only be grown from high boiling solvents,[7,8] but Infante-Castillo *et al*.[11] demonstrated on the basis of Raman spectra that α-RDX can undergo a solid-solid phase transition to β-RDX upon heating. Furthermore, Goldberg *et al.* performed a comprehensive investigation into crystal growth of β-RDX and demonstrated that the β-form can consistently be obtained from a wide range of solvents using the technique of drop-cast crystallization.[12]

Compression of the α-form to pressures exceeding 3.9 GPa at ambient temperature induces a phase transition to the γ-form, which has been structurally characterized by neutron powder diffraction and single crystal X-ray diffraction.[13] Vibrational studies at elevated pressures include Raman studies at ambient temperature which explored the effect of hydrostatic compression on the vibrational properties of both α- and γ-forms of RDX.[14,15] Ciezak & Jenkins[17] used spectroscopy to obtain a P-T phase diagram of RDX. Raman and far-infrared spectroscopic studies suggest a further high-pressure polymorph at pressures >17.8 GPa, denoted as the δ-form,[16,17] but the crystal structure of this δ-form is currently unknown. Millar *et al*. recently characterized a high-pressure/high-temperature polymorph, ε-RDX (obtained by compression of RDX through the α → γ

phase transition then heating to 448 K), using a combination of diffraction techniques.[18] The Raman spectra of ε-RDX have also been reported.[19,20]

A complementary approach to experiment is atomistic simulation, which provides an effective way to model the properties and structure of crystalline materials. The suitability of density functional theory (DFT) for studying energetic molecular materials has been reported in depth.[21,22,23] It is well known that conventional DFT methods cannot provide reliable results for intermolecular interactions in systems for which van der Waals (vdW) or dispersion interactions are the major component. Byrd *et al.* studied a series of energetic materials at ambient pressure and found poor agreement with experiment, with errors as high as 9.6% for the calculation of lattice parameters.[21] A subsequent study demonstrated that an increase in pressure diminishes the importance of the dispersion interactions relative to the increasing contribution of the repulsive interactions.[22] As the external pressure applied to the simulation cell increased, the inaccuracies of the predicted intermolecular distances and lattice parameters relative to experimental data decreased, to the extent that good agreement with experiment was produced for pressures greater than 6-7 GPa. [21,22]

Shimojo *et al.*[24] have shown that the dispersion correction implemented by Grimme[25] accounts for the dispersion interactions accurately for the α-RDX crystal in the high-pressure regime (0 – 15 GPa), while incurring little additional computational overhead. In addition, the authors determined that the non-empirical van der Waals density-functional (vdW-DF) method also provides an accurate description of the vdW interactions, but requires orders-of-magnitude more computational resource.[24] Similarly, Sorescu *et al.* performed theoretical predictions of the responses of the crystallographic lattice parameters to pressure for ten energetic molecular crystals, including the α- and γ-forms of RDX.[26] They concluded that the dispersion-corrected density functional theory method (DFT-D) as parameterized by Grimme[25] provides significant improvements for the

description of intermolecular interactions in molecular crystals at both ambient and high pressures relative to conventional DFT. Balu *et al.* investigated the performance of dispersion-corrected atom-centered pseudopotentials (DCACP's) at describing the ambient-pressure crystal structure of several energetic materials and demonstrated excellent agreement with experiment, giving results that were comparable to DFT-D studies.[27]

In this work we demonstrate the capability of the DFT-D functional parameterized by Grimme[25] to simulate accurately not just the structure, but also the vibrational and thermochemical properties of selected polymorphs of RDX. Furthermore, we provide the first experimental determination of the enthalpy of fusion of the highly metastable β-form of RDX, which provides further validation of the predictive capability of the computational method used in this study.

The organization of the paper is as follows. Section 2 describes the specific details of the experimental and computational methods used in this study. Section 3 presents the results of the computational predictions of ambient pressure structure, vibrational properties and lattice energies compared to corresponding experimental data, followed by experimental differential scanning calorimetry (DSC) results for the enthalpy of fusion of β-RDX. The predicted compression behaviors (equations-of-state and vibrational properties) are then analyzed for the α-, γ- and ε-forms of RDX, culminating in the prediction of the effect of elevated pressure on the heat capacities of RDX. The main conclusions of this work are summarized in Section 4.

2. Experimental and Computational methods

2.1 Computational methods

Structure optimizations (at ambient pressure and under hydrostatic externally applied pressure conditions) and vibrational frequency calculations were performed using density functional theory plus dispersion (DFT-D) coupled to the plane-wave pseudopotential method, as implemented in CASTEP version 5.5.[28] The dispersion correction scheme of Grimme[25] was utilized throughout. Treatment of electronic exchange and correlation was handled by the generalized gradient approximation (GGA) formalized by Perdew, Burke and Ernzerhof (PBE).[29] On-the-fly (OTF) [30] pseudopotentials were generated using CASTEP expressed at an energy cut-off of 700 eV, which ensured convergence of lattice parameters and total energies to less than 1 meV per atom. Brillouin zone sampling was obtained using Monkhorst-Pack[31] grids of 2 × 2 × 3, 2 × 3 × 2 and 3 × 2 × 2 for the α-, γ- and ε-polymorphs, respectively (all resulting in 2 *k*-points in the irreducible Brillouin zone). The structures were relaxed [using the Broyden, Fletcher, Goldfarb and Shannon (BFGS)[32] method] to allow both atomic coordinates and unit cell vectors to optimize simultaneously while constraining space group geometry. The following convergence criteria were applied: maximum change in system energy = 2 x 10^{-5} eV, maximum root-mean-square (RMS) force = 0.025 eV $Å^{-1}$, maximum RMS stress = 0.01 GPa and maximum RMS displacement = 0.002 Å. Following successful geometry optimization, external hydrostatic pressures were applied at pressures corresponding to the available experimental data. Phonon frequencies (at the gamma point in *k*-space) for the optimized structures were then calculated by finite displacement methods.[33]

In order to create potentials wells to determine lattice energies, single-point energy (SPE) calculations were performed on the experimental structure of α-RDX using both DFT and DFT-D methods. Further SPE calculations on structures with smaller/larger volumes were performed by

isotropically decreasing/increasing the experimental lattice parameters. The preceding methodology was then repeated for the crystal structure of β-RDX.

2.2 Inelastic Neutron Scattering (INS)

INS spectra (24-4000 cm^{-1}) were recorded using the TOSCA[34] instrument at the ISIS Neutron and Muon Facility, which has an energy resolution of ~1.25% of the energy transfer. Approximately 4.0 g of polycrystalline α-RDX (Bridgwater Type I, Class 5 ~ 10-30 μm) was loaded into an aluminum sample can and cooled to T < 20 K in a conventional closed cycle refrigerator. Spectra were recorded for 3–6 h. INS data were visualised and compared to the simulated spectra of the DFT-D calculations using the aCLIMAX program.[35]

2.3 Differential Scanning Calorimetry (DSC)

Samples of α-RDX (Bridgwater Type I, Class 5 ~ 10-30 μm) were loaded into aluminum pans (TA Instruments Tzero™ series) and hermetically sealed and weighed (0.153 – 0.261 mg). β-RDX was obtained by crystallization from the melt. Thermograms were obtained on a TA Instruments Q2000 DSC module with heat flow recorded using a Tzero™ cell. The apparatus was calibrated using indium. Measurements were performed from 20 °C to 215 °C with a heating rate of 10 °C min^{-1}. A helium gas flow of 50 ml min^{-1} was maintained through the furnace during measurements. The resulting DSC traces were analyzed by means of the TA Universal Analysis Software.

2.4 X-Ray Powder Diffraction

Samples of α-RDX (Bridgwater Type I, Class 5 ~ 10-30 μm) were densely packed into 0.7 mm diameter thin-walled glass capillaries. X-ray powder diffraction data were collected on Beamline I11 (HRPD) at the Diamond Light Source (λ = 0.826136(2) Å).[36,37]

3. Results and discussion

3.1 Ambient-pressure behavior

3.1.1 Structure and spectroscopic properties of α-RDX

α-RDX crystallizes in the orthorhombic crystal system with space group *Pbca*: the unit cell contains eight RDX molecules, giving a total of 168 atoms. The ambient-pressure structure of α-RDX has been previously calculated with good accuracy; our results are included here purely to demonstrate that we have also successfully reproduced the experimentally observed parameters, in order to give confidence to the further computational work which follows. The results of the geometry optimization compared to available experiment and previous DFT and DFT-D studies are shown in **TABLE 1** (TABLE S1 of the supplementary information presents a full comparison of the DFT-D calculated and experimental room temperature crystallographic parameters at ambient and elevated hydrostatic pressures). All lattice parameters agree with experiment to within 1.3%, and the overall unit cell volume differs from experiment by only 0.3 %. These results are consistent with previous DFT-D studies,[24,26] and confirm that the Grimme dispersion correction can accurately describe the intermolecular interactions in the α-RDX crystal.

Following the geometry optimization, a comprehensive, finite displacement phonon calculation (including symmetry) was performed to obtain the vibrational properties of α-RDX. Due to the large number of calculated and experimental modes a detailed comparison has not been presented here. However, a full list of calculated vibrational modes with experimental comparisons from both Haycraft *et al*[5] and Dreger & Gupta[14] can be found in TABLE S2 of the supplementary information. The majority of the calculated Raman-active vibrational modes are in good agreement (<2.5 % difference) with experiment.

The simulation also agrees very well with the INS spectrum obtained during the course of this work. Our INS spectrum is, in turn, in good agreement with previously published INS experiments performed on α-RDX by Ciezak *et al.* (43 – 1299 cm^{-1}), and extend the wavenumber range for these measurements (24 – 4000 cm^{-1}). INS spectra provide a unique way to assess the quality of the computational phonon calculations. This is because the eigenvalues of a vibration are a function of the molecule's structure and the intramolecular forces, and correspond to the energies lost by the neutron. Furthermore, the intensity of the observed transition is a function of the eigenvector and the momentum lost by the neutron.[38] Thus by comparing calculated spectra to INS spectra it is possible to assess how well both the wavenumber and eigenvector of each mode are calculated. In **Figure 2** the calculated INS spectra of α-RDX calculated using DFT-D is compared to the ambient-pressure experimental INS spectra recorded using the TOSCA instrument.[34] From this it is apparent that the computed and experimental spectra show excellent agreement, both for the transition energies and for the intensities of the lattice and internal modes.

The excellent agreement between experiment and theory for the crystallographic lattice parameters and for the vibrational frequencies and intensities gives confidence that the computational model used in this study accurately describes both the intramolecular and intermolecular interactions in crystalline α-RDX.

3.1.2 Calculation of lattice energies of α- and β-RDX

The lattice parameters of the experimental crystal structure of α-RDX were isotropically increased and decreased, ensuring that the intramolecular distances *i.e.* bond lengths and angles of the molecules in the crystal were left unchanged while the intermolecular distances were increased / decreased with changing unit cell size. Single-point energy calculations were performed on a range of cell sizes; potential wells were constructed by plotting the calculated energy difference (E_0-E) of

the smaller/larger volume crystal structures against V/V_0, where V_0 and E_0 are the energy and unit-cell volume of the experimental crystal structure, respectively. The resulting potential wells were fitted with Lennard-Jones type potentials of the form shown in **Equation 1**:

$$y = 4A\left(\left(\frac{B}{x}\right)^C - \left(\frac{B}{x}\right)^D\right) + E \quad (1)$$

Where, *A*-*E* are free variables. Thus the lattice energy E_L (here defined to be negative) can be calculated from the difference in energy between the base of the well and the calculated variable *E* (*i.e.* the point at which the potential well levels off) divided by the number of molecules in the unit cell. In this study, zero point energy contributions have been neglected.

A schematic diagram of the potential wells, along with the corresponding information that can be taken from it, is shown in **Figure 3**.

Figure 4 shows the calculated potential wells obtained for α-RDX using DFT and DFT-D methods, and the potential well obtained using the DFT-D method for the β-form of RDX.

The sublimation enthalpy is the difference between the enthalpies in the gaseous and solid states, as given by **Equation 2**.

$$\Delta H_{sub} = H_{gas} - H_{solid} \quad (2)$$

Assuming that the gas is ideal and that the Dulong-Petit Law holds for the solid then each degree of freedom contributes ½ RT to the enthalpy of the system. Thus as there are three translational and three rotational kinetic degrees of freedom, H_{gas} is given by **Equation 3**, where the final RT term accounts for PV (in accordance with the ideal gas law).

$$H_{gas} = \frac{3}{2}RT + \frac{3}{2}RT + RT \quad (3)$$

In the solid state, there are three degrees of freedom for both kinetic and potential energy components of the translational and librational oscillations, in addition to the intramolecular component of internal energy (the lattice energy, E_L). Thus H_{solid} is given by **Equation 4**:

$$H_{solid} = 3RT + 3RT + E_L \quad (4)$$

It follows that by inserting **Equation 3** and **Equation 4** into **Equation 2**, that the lattice energy, E_L, can be related to the enthalpy of sublimation, ΔH_{sub}, by **Equation 5**.

$$-E_L = \Delta H_{sub} + 2RT \quad (5)$$

However, due to the nature of the experimental methods used to determine enthalpies of sublimation, the absolute temperatures at which ΔH_{sub} are measured are often unknown. As a result, the relationship above is often simplified to that shown in **Equation 6**, in order to compare calculated lattice energies to experimentally determined sublimation enthalpies. [39,40,41,42,43,44]

$$-E_L \approx \Delta H_{sub} \quad (6)$$

The enthalpy of sublimation for α-RDX has been independently determined experimentally by Rogers[45] to be 130.12 kJ mol^{-1} and by Rosen *et al.*[46] to be 130.16 kJ mol^{-1}. As stated above, in this paper we directly compare calculated E_L and the experimentally determined ΔH_{sub} (as shown by Equation 6) but it should be noted that a correction of a few kJ mol^{-1} has been neglected in order to be able to make this approximation.

In **TABLE 2** the lattice energies for α-RDX calculated using DFT and DFT-D methods are compared to the experimentally determined enthalpies of sublimation. DFT seriously underestimates the lattice energy of α-RDX, again demonstrating that this model cannot accurately describe the intermolecular interactions within crystalline RDX. By contrast, E_L calculated using DFT-D (-130.06 kJ mol^{-1}) is in excellent agreement with experiment. Previous calculations by Perger *et al,*.[47] investigated the predictive power of multiple functionals with differing basis sets and

different levels of theory and showed that both HF and DFT-GGA methods significantly underestimate the lattice energy (HF: 40.4 – 65.0 kJ mol^{-1}, B3LYP: 36.3 – 43.1 kJ mol^{-1}, GGA: 57.8 – 63.3 kJ mol^{-1}). Hu *et al*.[48] and Wang *et al*.[49] both calculated the enthalpy of sublimation of α-RDX, with predictions of 109.7 and 100.4 kJ mol^{-1}, respectively. The most accurate prediction to date was obtained using the COMPASS force field, which predicted the lattice energy of α-RDX to be -116.7 kJ mol^{-1}.[50]

The successes of the DFT-D approach prompted us to calculate E_L for β-RDX (the calculated potential well is shown in **Figure 4**, with parameters from the Lennard-Jones type fit shown in **TABLE 2**, giving a predicted lattice energy of -109.71 kJ mol^{-1}). Thus we would expect the experimental E_L (ΔH_{sub}) of β-RDX to be approximately 20 kJ mol^{-1} more positive than that of α-RDX. This is an unusually large difference between polymorphs of a molecular crystal – energy differences are typically less than 10 kJ mol^{-1}.[51,52,53] However, this is by no means the first observation of a large energy difference between polymorphs; the drug Efavirenz ((4*S*)-6-chloro-4-cyclopropylethynyl-4-trifluromethyl-1,4-dihydro-2*H*-3,1-benzoxazin-2-one) crystallizes in multiple polymorphic forms, and recent DSC experiments have shown that the enthalpies of fusion of these different forms vary considerably, the difference between Form I and Form III being over 17 kJ mol^{-1}.[54] Similarly, studies on a simple N, N'- diaryl urea derivative (1-(3-Methylsulfanylphenyl)-3-pyridin-2-ylurea) determined a difference in the enthalpies of fusion of 23.4 kJ mol^{-1} between the thermodynamically stable Form IV and the metastable Form I.[55]

3.1.3 Experimental determination of enthalpy of fusion of β-RDX

The enthalpy of fusion of α-RDX has been previously experimentally determined using DSC by Hall (35.65 ± 2.51 kJ mol^{-1}),[56] Kishore (30.71 ± 0.29 kJ mol^{-1}),[57] and Zeman (32.90 ± 0.73 kJ mol^{-1}).[58]

The challenge in measuring ΔH_{fus} for β-RDX is the high degree of metastability, illustrated by the observation that any mechanical manipulation of the β-form results in immediate transformation to the α-form.[8,12] The β-form can be reproducibly obtained by drop-cast recrystallization, *i.e*. evaporation of dilute solutions of RDX in solvents such as DMSO. In this way Goldberg *et al*. obtained DSC traces for the β-form and identified its melting temperature as 188 °C, but did not report its enthalpy of fusion.[12] The authors also commented on the influence of scale on the crystallization of the β-form - crystallization of samples from higher concentration drops increased the propensity for the α-form to crystallize.[12]

Our approach was to crystallize the β-form from the melt, first using X-ray powder diffraction to identify unequivocally that the β-form is formed in this way. To this end powder diffraction patterns of the α-form contained in a 0.7 mm thin-walled glass capillary were recorded until just before the melting point (477 K) – all were consistent with the α-form. It was only after complete melting of the sample and cooling to ambient temperature that the characteristic diffraction pattern of the β-form was obtained, albeit with very pronounced preferred orientation which affects the observed intensities (see **Figure 5**). This contrasts somewhat from the results of Infante-Castillo *et al*., who reported that the α → β transition occurred *via* a solid-solid transition, but this may be a consequence of the different methods of containment of the sample in the two experiments. Nevertheless, it did prove possible to obtain samples of the β-form in a reproducible manner by cooling from the melt, and so this was the strategy adopted for the DSC experiments in this work. To this end, a sample of α-RDX was first heated in a sealed aluminum pan to just beyond the melting point of the α-form (204 °C) and then cooled to ambient temperature. However, initial experiments using quantities of 2-3 mg of RDX were unsuccessful – invariably only the α-form crystallized. It was only when samples of mass <~0.25 mg were used that reproducible

crystallization of the β-form could be achieved. Thus crystallization of the β-form from the melt also appears to be strongly affected by scale in a similar way to the drop-cast recrystallization of RDX from solution.[12]

A typical DSC thermogram obtained for β-RDX is shown in **Figure 6** (all other thermograms that were recorded can be found in the supplementary information, Figures S1-S4). Upon heating from 20 °C to 210 °C an endothermic peak was observed with an onset temperature of 186.7 ± 0.8 °C, indicative of melting of the β-form, and in agreement with the results of Goldberg *et al*.[12]

The observed characteristics of fusion determined for five samples of β-RDX are shown in **TABLE 3**. From this sample set, the mean and standard deviation for the onset temperature (or melting point), peak temperature and ΔH_{fus} have been determined as 186.7 ± 0.8 °C, 188.5 ± 0.4 °C and 12.63 ± 0.28 kJ mol^{-1}, respectively. This represents the first experimental determination of the enthalpy of fusion of β-RDX.

A pertinent comparison between the calculated lattice energies and experimentally determined data can be obtained by comparing the difference between the calculated lattice energies with the difference in experimentally determined enthalpies of fusion for α- and β-RDX, for in this way any errors due to the omission of zero-point energy corrections will cancel. This gives a value of 20.35 kJ mol^{-1} from the simulations, compared to 20.46 ± 0.92 kJ mol^{-1} obtained from the difference between the experimental ΔH_{fus} of β-RDX (determined in this study) and the average of the literature values quoted above for ΔH_{fus} of α-RDX (33.086 ± 0.877 kJ mol^{-1}).

With a knowledge of this difference in the enthalpies of fusion, we can subtract this from the enthalpy of sublimation of α-RDX, to determine the 'experimental' lattice energy of β-RDX as -109.68 ± 1.27 kJ mol^{-1}. The lattice energy of β-RDX predicted earlier in this study by DFT-D (-

109.71 kJ mol^{-1}) is in excellent agreement with this experimental determination, which serves to highlight the predictive power of a good computational model.

These experimental findings may have considerable implications for polymorph prediction strategies,[59] where large numbers of possible structures are generated, and those that are not within ~10 kJ mol^{-1} of the lowest energy structure are typically discarded. The observed β-RDX polymorph in this study would be overlooked in such a screening, highlighting that care must be taken when choosing selection criteria in some polymorph prediction studies.

3.2 High-pressure behavior of the α- γ- and ε-forms of RDX

3.2.1 Effect of pressure on lattice parameters

Although the structures of the α- and γ-forms of RDX as a function of pressure have been previously calculated with good accuracy, we briefly present the results of our findings as validation of the calculated high-pressure vibrational properties and ultimately the calculated heat capacities at elevated pressures. The effect of pressure on the lattice parameters of the α- and γ-forms of RDX is shown in Figures S5 and S6 in the supplementary information. The results are in very close agreement with a previous computational DFT-D study,[26] and are in excellent agreement with experiment over the pressure range.[60] Lattice parameters are calculated to lie within 1.6 % and 1.1 % (for α-RDX and γ-RDX respectively) of the experimental values determined by Oswald *et al*.[60] and all unit-cell volumes for α-RDX are calculated to within 1.3 % of experiment, with the largest deviation from the experimental γ-RDX volume being just 0.9 %.

3.2.2 Compression of ε-RDX

This work presents the first computational compression study of the recently characterised high-temperature/high-pressure polymorph, ε-RDX. **Figure 7** shows that the experimental[10] lattice parameters and compression behaviour are reproduced well by the DFT-D method. The *a*-axis is

consistently overestimated by ~1 %, the *b*-axis is initially overestimated by 0.5 %, and upon compression the overestimation gradually rises, with a maximum difference of 1.3 % at 4.64 GPa. Calculation of the *c*-axis is initially underestimated by 1.8 % at 0.99 GPa but as the pressure is increased the difference compared to experiment decreases to only 1.0 % at 5.04 GPa, the maximum pressure of the experimental study.

Figure 8 depicts the overall unit cell volume compression as a function of pressure for ε-RDX. The compression results are compared to experiment[10] and are fitted to a Murnaghan[61] equation-of-state. The unit-cell volumes as a function of pressure for ε-RDX were calculated in excellent agreement with experiment, with deviations of no more than 0.9 % over the pressure range studied.

Calculated equations of state (EoS), presented in **TABLE 4**, highlight the quality of the simulated results. Results obtained for all three polymorphs are shown alongside their experimentally-derived counterparts, along with available results by Sorescu and Rice. It can be seen that both this work and the DFT-D calculations by Sorescu and Rice[26] slightly overestimate the compressibility of α-RDX. This is primarily due to the initial underestimation of the unit cell volume at ambient pressure for both computational studies, in conjunction with the subsequent slight overestimation at elevated pressures. However, for both γ- and ε-RDX, the computational models in this work generate B_0 values in excellent agreement with experiment.

3.2.3 High-pressure vibrational properties

High-pressure vibrational mode calculations have also been performed for α-, γ- and ε-RDX. Due to experimental limitations, it has not been possible to obtain experimental INS spectra for γ- and ε-RDX. However, the calculated high-pressure vibrational properties of α-, γ- and ε-RDX are compared to available high-pressure Raman spectra published by Dreger & Gupta.[14,19] The results of the high-pressure phonon calculations, and corresponding experimental values for α-RDX, can be

found in TABLE S2 of the supplementary information; TABLES S5 and S6 present the results for γ- and ε-RDX, respectively. This shows that the computational model appears to be capable of reliably predicting the vibrational properties of the polymorphs of RDX over a range of pressures. Computed INS spectra for γ- and ε-RDX, compared to the computed spectra of α-RDX at similar pressures, can be found in the supplementary information in Figures S7 & S8.

3.2.4 Prediction of heat capacities

The successes of the DFT-D model for the prediction of lattice energies, compression behaviour and vibrational properties of RDX, give confidence that the model is capable of predicting properties that have not yet been experimentally measured. Hence, by utilizing the results of the phonon calculations, we have predicted the variation in heat capacities as a function of pressure for the α-, γ- and ε-forms of RDX. These results provide insight into the requirements of potential experimental techniques for measuring heat capacities at elevated pressure.

The heat capacity at a given pressure can be calculated using **Equation 7**:

$$C_{V,tot} = \frac{3}{2}R + 0 + \frac{3}{2}R + R\sum_{\kappa}\frac{\left(\frac{\Theta_{v,\kappa}^2}{T^2}\right)e^{\frac{\Theta_{v,\kappa}}{T}}}{\left(e^{\frac{\Theta_{v,\kappa}}{T}}-1\right)^2} \quad (7)$$

Where the four terms represent the contributions from the translational, electronic, rotational and vibrational partition functions respectively. $\Theta_{v,\kappa}$ is the vibrational temperature of each mode, κ, given by **Equation 8**:

$$\Theta_{v,\kappa} = \frac{h\nu_{\kappa}}{k_B} \quad (8)$$

Where h is Planck's constant, ν_{κ} is the computed phonon frequency and k_B is the Boltzmann constant.

Figure 9 displays the calculated variation in heat capacities at 295 K in the 0 – 8 GPa pressure range for α-, γ- and ε-RDX. The calculated heat capacity for α-RDX at ambient pressure at this temperature is 216.17 J K^{-1} mol^{-1} , close to the experimental value of 231.68 J K^{-1} mol^{-1} determined by Miller.[62] **Figure 9** shows that the effect of pressure on the heat capacities for all three polymorphs is only approximately -1 J K^{-1} mol^{-1} GPa^{-1} (in comparison to a temperature dependence of approximately 0.6 J K^{-1} mol^{-1} for α-RDX[62,63]). In addition, at the α-γ phase transition the discontinuity is only 0.25 J K^{-1} mol^{-1}. These results illustrate that there is a weak pressure dependence of heat capacities for all three forms of RDX studied here. Thus to determine experimentally the effect of pressure on the heat capacities of materials such as RDX, a very sensitive method will be needed. Furthermore, these results highlight that pressure does not play a major role in influencing the deflagration-to-detonation transition; instead the major influence is temperature as heat capacities are highly temperature dependent.

4. Conclusions

DFT-D calculations have been utilized to describe accurately the structure and properties of several polymorphs of the organic molecular crystal RDX. At ambient pressure the DFT-D model predicted all of the lattice parameters of α-RDX to within 1.3 % of experiment,[2] commensurate with previous DFT-D studies.[24,26] Subsequent phonon calculations generated vibrational frequencies in good agreement with experimental Raman spectra. From the results of the phonon calculation an INS spectrum was plotted and compared with the experimental spectrum. Eigenvalues and eigenvectors were well replicated by the model. The lattice energy of α-RDX was calculated to be -130.06 kJ mol^{-1}, in excellent agreement with the experimental ΔH_{sub} value of 130.14 kJ mol^{-1}. The good agreement between theory and experiment for α-RDX prompted use of the DFT-D model to predict the lattice energy of the metastable β-form of RDX (-109.71 kJ mol^{-1}) and this was found to be 20.35 kJ mol^{-1} more positive than for α-RDX. As part of the study we also performed the first experimental determination of the enthalpy of fusion, ΔH_{fus}, of the highly metastable β-RDX. The characteristics of fusion for β-RDX were determined to be 186.7 ± 0.8 °C, 188.5 ± 0.4 °C and 12.63 ± 0.28 kJ mol^{-1} for the onset temperature (or melting point), peak temperature and ΔH_{fus}, respectively. The difference in experimental ΔH_{fus} for the α- and β-forms of RDX is 20.46 ± 0.92 kJ mol^{-1}, in excellent agreement with the computationally predicted difference in lattice energies. These findings may have considerable implications for polymorph prediction strategies, where structures not within ~10 kJ mol^{-1} of the lowest energy structure are typically discarded. The observed β-RDX polymorph in this study would be overlooked in such a screening, highlighting that care must be taken when choosing selection criteria in some polymorph prediction studies.

The high-pressure behavior of RDX was also investigated. DFT-D hydrostatic compression studies included the α- and γ-forms of RDX, with structures produced that were in good agreement with experiment,[60] and a previous DFT-D study.[26] Moreover the first computational study of the recently characterized ε-form of RDX has been performed. The experimental high-pressure behaviour of ε-RDX was reproduced well by the computational model, with the calculated bulk modulus (10.63 GPa) in excellent agreement with the experimentally determined value of 10.34 ± 1.74 GPa. The vibrational properties as a function of pressure were calculated for the α-, γ- and ε-forms of RDX, and were found to be in very good agreement with available experimental data. The results of the phonon calculations were then used to predict the effect of pressure on the heat capacities of the α-, γ- and ε-forms of RDX. These predictions suggest a very weak pressure dependence of heat capacities for all crystal forms of RDX, and in particular highlighted the very small (0.25 J K^{-1} mol^{-1}) discontinuity at the α-γ phase transition. Thus, elevated pressures do not significantly affect the specific heat capacity of RDX and so the small pressure-induced changes in heat capacity do not play a significant role in the rate of deflagration nor the DDT. In addition, these results indicate that the experimental determination of the effect of pressure on the heat capacities of materials such as RDX is likely to be a very challenging task, and would require the use of a very sensitive technique.

This comprehensive study of selected polymorphic forms of crystalline RDX at ambient and applied high-pressures has shown that the DFT-D model performs extremely well over a range of conditions, and is able to describe accurately intramolecular and intermolecular interactions and thus the structure and properties of the organic molecular crystal RDX.

5. Acknowledgments

We gratefully acknowledge Dr. Philip J. Camp (The University of Edinburgh) for helpful discussions. We thank the Scottish Funding Council (SPIRIT) and QinetiQ (in support of MOD research) for contribution towards a studentship (SH); the ESPRC for the provision of high-performance computing time and The Department of Materials Science, University of Cambridge for use of the DSC module. This work made use of the facilities of HECToR, the UK's national high-performance computing service, which is provided by UoE HPCx Ltd at the University of Edinburgh, Cray Inc and NAG Ltd, and funded by the Office of Science and Technology through EPSRC's High End Computing Programme. We acknowledge the support of the Diamond Light Source, STFC, and the ISIS Neutron and Muon Facility.

6. Supporting Information Available

The remaining DSC thermograms for β-RDX can be found in Figures S1-S4. Figures S5 and S6 display a comparison between the calculated lattice parameters and unit cell volumes for α- and γ-RDX, compared to previous DFT-D studies as well as relevant experimental data. Figures S7 and S8 compare predicted INS spectra for α-RDX to those for γ- and ε-RDX at similar pressures. Tables S1, S3 and S4 display a comparison of the DFT-D predicted crystallographic parameters with corresponding experimental data for α-, γ- and ε-RDX respectively. Full lists of calculated phonon modes as a function of pressure for α-, γ- and ε-RDX compared to experimental Raman data, including pressure-induced shift values can be found in Tables S2, S5 and S6. This information is available free of charge via the Internet at http://pubs.acs.org

7. Figure Captions

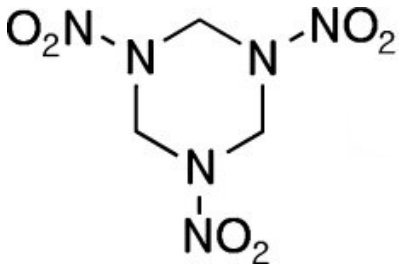

Figure 1 Structure of RDX.

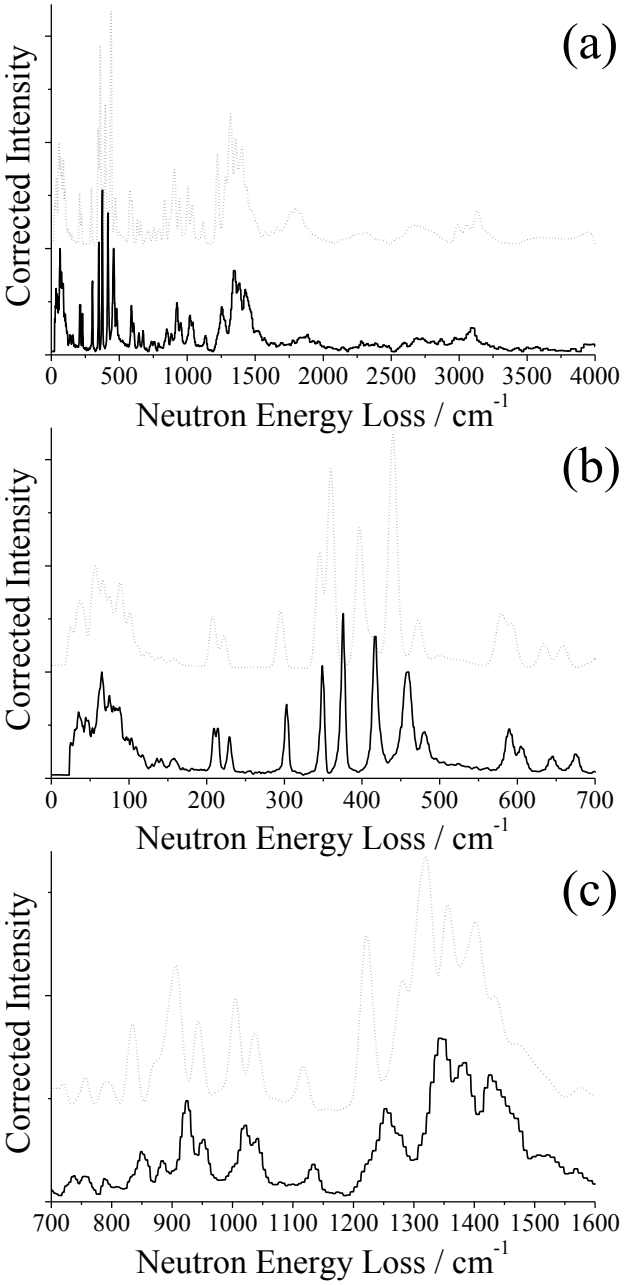

Figure 2 Experimental (solid line) and calculated (dotted line) INS spectra of α-RDX at ambient pressure in the regions (a) 0 – 4000 cm^{-1}, (b) 0 – 700 cm^{-1}, (c) 700 – 1600 cm^{-1}.

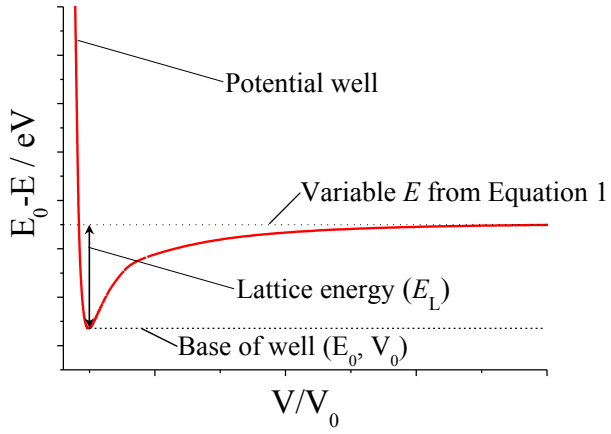

Figure 3 Schematic diagram of potential well used to fit **Equation 1** to give lattice energies.

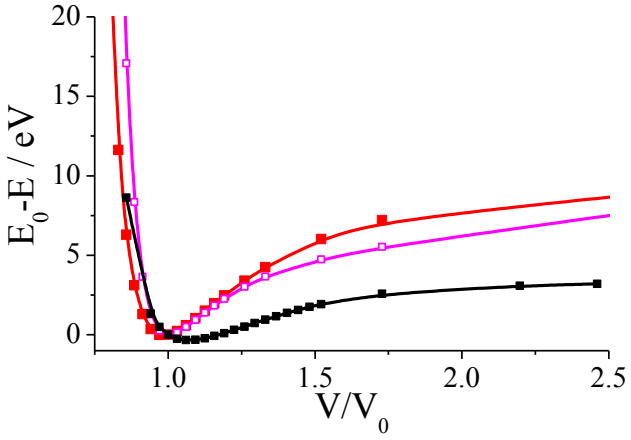

Figure 4 Calculated potential wells for α- and β-RDX fitted with Lennard-Jones type potentials. —■— α-RDX DFT, —■— α-RDX DFT-D and, —□— β-RDX DFT-D.

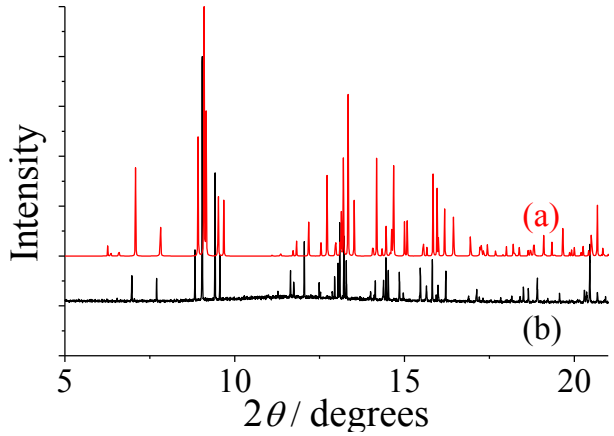

Figure 5 Powder X-ray diffraction patterns of (a) RDX recrystallised from the melt and then cooled to 298 K and (b) simulated powder pattern of the single crystal X-ray diffraction structure of β-RDX at 150 K. (λ = 0.826136(2) Å)

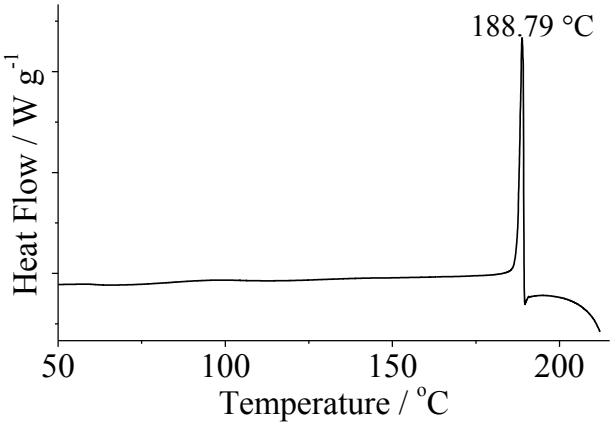

Figure 6 Typical DSC thermograph, obtained at a heating rate of 10 °C per minute for β-RDX (sample mass 0.153 mg).

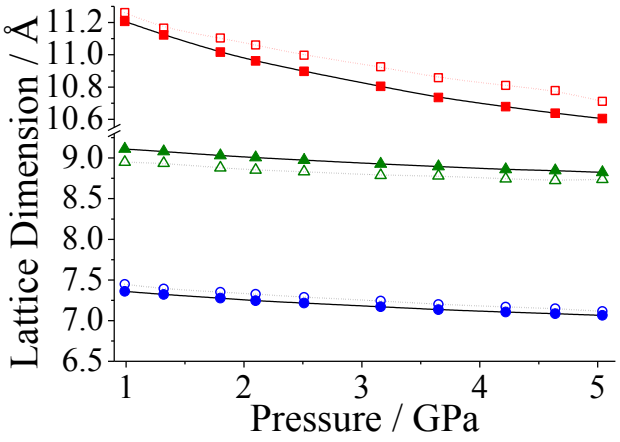

Figure 7 Variation of lattice parameters as a function of hydrostatic pressure for crystalline ε-RDX. —●— *a*- , —■— *b*- and, —▲— *c*- vectors (solid symbol: experimental,[10] open symbol: computational).

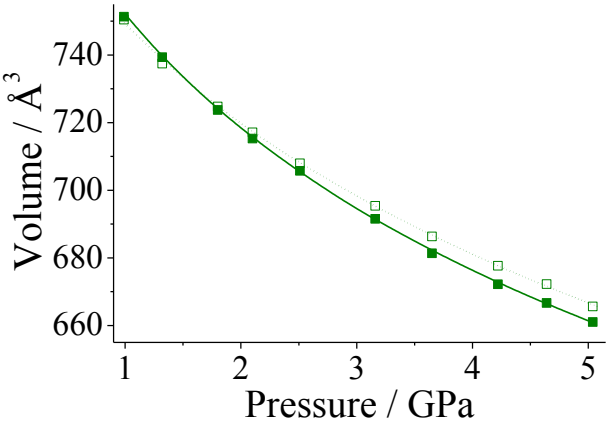

Figure 8 Unit cell volumes as a function of pressure for ε-RDX, fitted to Murnaghan equations of state (solid symbol: experimental,[10] open symbol: computational).

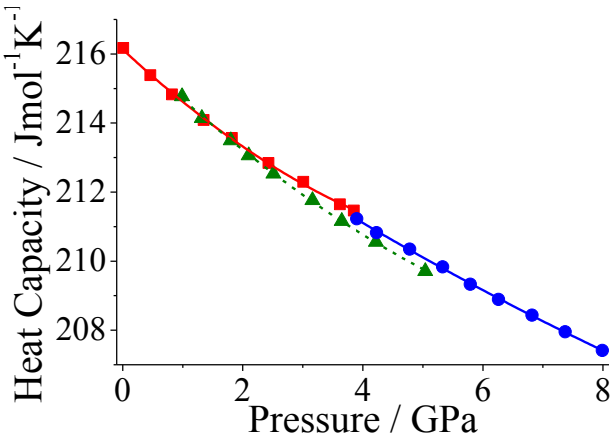

Figure 9 Calculated effect of pressure on the heat capacities at T= 295 K of α-RDX (■), γ-RDX (●) and ε-RDX (▲).

8. Tables

TABLE 1 Comparison of the crystallographic parameters for α-RDX calculated at ambient pressure using the DFT-D method alongside results obtained from ambient temperature experimental and previous DFT and DFT-D studies. The numbers in square brackets are the estimated standard deviations of experimental values, the values in parentheses are the percentage error deviations from experimental values.

Parameter	**Exp.**[2]	**DFT**[22]	**DFT-D Sorescu & Rice**[26]	**DFT-D (This work)**
a (Å)	13.182[2]	13.688 (3.8)	13.237 (0.4)	13.282 (0.8)
b (Å)	11.574[2]	11.933 (3.1)	11.391 (-1.6)	11.419 (-1.3)
c (Å)	10.709[2]	11.538 (7.7)	10.770 (0.6)	10.736 (0.3)
V (Å^3)	1633.86[5]	1884.52 (15.3)	1623.94 (-0.6)	1628.27 (-0.3)

TABLE 2 Calculated lattice energies of α-RDX using both DFT & DFT-D methods compared to experimental heats of sublimation, along with the predicted lattice energy for β-RDX.

	E **(derived from Eq 1) (eV)**	E_L **(kJ mol^{-1})**	ΔH_s **(kJ mol^{-1})**
α-RDX DFT	3.992	-48.15	
α-RDX DFT-D	10.784	-130.06	
α-RDX Exp.[45]			130.12
α-RDX Exp.[46]			130.16
β-RDX DFT-D	9.097	-109.71	

TABLE 3 Observed characteristics of fusion for β-RDX samples.

Mass (mg)	**Onset T (°C)**	**Peak T (°C)**	**Peak area (J g^{-1})**	**$\Delta H°_{fus}$ (kJ mol^{-1})**
0.153	187.5	188.8	58.66	13.02
0.184	186.4	188.8	55.99	12.44
0.184	186.2	188.1	56.65	12.58
0.194	185.8	188.0	55.48	12.32
0.261	187.5	188.9	57.50	12.77
Mean	**186.7 ± 0.8**	**188.5 ± 0.4**	**56.86 ± 1.26**	**12.63 ± 0.28**

TABLE 4 Experimental and calculated 3rd order Birch-Murnaghan (α-RDX and γ-RDX) and Murnaghan (ε-RDX) equation of state parameters of crystalline RDX.

		V_0 / Å^3	**B_0 / GPa**	**B'**
α-RDX	Exp.[60]	1639.8 (5.8)	10.10 (1.18)	11.00 (1.65)
	DFT-D	1630.7 (3.7)	15.54 (1.08)	6.46 (0.82)
	Ref. 26	1625.6	13.99	7.80
γ-RDX	Exp.[60]	1616.1 (8.0)	9.50 (0.41)	11.00 (fixed)
	DFT-D	1616.1 (fixed)	9.17 (0.20)	12.63 (0.36)
	Ref. 26	1555.0	16.72	8.03
ε-RDX	Exp.[10]	808.3 (7.6)	10.34 (1.74)	7.78 (0.65)
	DFT-D	799.3 (6.4)	10.63 (2.25)	12.32 (2.51)

References

[1] Hakey, P.; Ouellette, W.; Zubieta, J.; Korter, T. Redetermination of Cyclo-trimethylene-trinitramine. *Acta Crystallogr., Sect. E: Struct. Rep. Online* **2008**, *64,* o1428.

[2] Choi, C. S.; Prince, E. The Crystal Structure of Cyclotrimethylene-trinitramine. *Acta Crystallogr., Sect. B: Struct. Crystallogr. Cryst. Chem.* **1972**, *28(9)*, 2857–2862.

[3] Rey-Lafon, M.; Trinquecoste, C.; Cavagnat, R.; Forel, M. T. Study of the Vibrational Spectra of Trinitro-1,3,5-hexahydro-s-triazine. I. Analysis of Infrared and Raman Spectra Between 3200 and 200 cm^{-1}. *J. Chim. Phys. Phys.-Chim. Biol*. **1971**, *68*, 1533–1542.

[4] Rey-Lafon, M.; Trinquecoste, C.; Cavagnat, R.; Forel, M. T. Study of the Vibrational Spectra of Trinitro-1,3,5-hexahydro-s-triazine. II. Analysis of Monocrystal Spectra Between 200 and 10 cm^{-1}. *J. Chim. Phys. Phys.-Chim. Biol.* **1971**, *68*, 1573–1577.

[5] Haycraft, J. J.; Stevens, L. L.; Eckhardt, C. J. Single-Crystal, Polarized, Raman Scattering Study of the Molecular and Lattice Vibrations for the Energetic Material Cyclotrimethylene-trinitramine. *J. Appl. Phys.* **2006**, *100(5)*, 053508-1–053508-9.

[6] Ciezak, J. A.; Trevino, S. F. Inelastic Neutron Scattering Spectrum of Cyclotrimethylenetrinitramine: A Comparison with Solid-State Electronic Structure Calculations. *J. Phys. Chem. A* **2006**, *110*, 5149–5155.

[7] McCrone, W. C. Crystallographic Data. 32. RDX (Cyclotrimethylenetrinitramine). *Anal. Chem.* **1950**, *22*, 954–955.

[8] Karpowicz, R. J.; Serglo, S. T.; Brill, T. B. ,β Polymorph of Hexahydro-1,3,5-trinitro-s-triazine. A Fourier Transform Infrared Spectroscopy Study of an Energetic Material. *Ind. Eng. Chem. Prod. Res. Dev*. **1983**, *22(2)*, 363–365.

[9] Karpowicz, R. J. Brill, T. B. Comparison of the Molecular Structure of Hexahydro-1,3,5-trinitro-s-triazine in the Vapor, Solution, and Solid Phases. *J. Phys. Chem*. **1984**, *88(3)*, 348–352.

[10] Millar, D. I. A.; Oswald, I. D. H.; Barry, C.; Francis, D. J.; Marshall, W. G.; Pulham, C. R.; Cumming, A. S. The Crystal Structure of β-RDX – an Elusive Form of an Explosive Revealed. *Chem. Commun.* **2009**, *5*, 562–564.

[11] Infante-Castillo, R.; Pacheco-Londoño, L. C.; Hernández-Rivera, S. P. Monitoring the α → β Solid–Solid Phase Transition of RDX with Raman Spectroscopy: A Theoretical and Experimental Study. *J. Mol. Struct*. **2010**, *970*, 51–58.

[12] Goldberg, I. G.; Swift, J. A. New Insights into the Metastable β Form of RDX. *Cryst. Growth Des*. **2012**, *12(2)*, 1040–1045.

[13] Davidson, A. J.; Oswald, I. D. H.; Francis, D. J.; Lennie, A. R.; Marshall, W. G.; Millar, D. I. A.; Pulham, C. R.; Warren, J. E.; Cumming, A. S. Explosives Under Pressure – the Crystal Structure of γ-RDX as Determined by High-Pressure X-ray and Neutron Diffraction. *CrystEngComm* **2008**, *10(2)*, 162–165.

[14] Dreger, Z. A.; Gupta, Y. M. High Pressure Raman Spectroscopy of Single Crystals of Hexahydro-1,3,5-trinitro-1,3,5-triazine (RDX). *J. Phys Chem B* **2007**, *111(15)*, 3893–3903.

[15] Zheng, X.; Zhao, J.; Tan, D.; Liu, C.; Song, Y.; Yang, Y. High-Pressure Vibrational Spectroscopy of Hexahydro-1,3,5-Trinitro-1,3,5-Triazine (RDX). *Propell. Explos. Pyrotech*. **2011**, *36*, 22–27.

[16] Ciezak, J. A.; Jenkins, T. A.; Liu, Z.; Hemley, R. J. High-Pressure Vibrational Spectroscopy of Energetic Materials: Hexahydro-1,3,5-trinitro-1,3,5-triazine. *J. Phys. Chem. A* **2007**, *111(1)*, 59–63.

[17] Ciezak, J. A.; Jenkins, T. A. The Low-Temperature High-Pressure Phase Diagram of Energetic Materials: I. Hexahydro-1,3,5-trinitro-s-triazine. *Propell. Explos. Pyrotech.* **2008**, *33(5)*, 390–395.

[18] Millar, D. I. A.; Oswald, I. D. H.; Barry, C.; Francis, D. J.; Marshall, W. G.; Pulham, C. R.; Cumming, A. S. Pressure-Cooking of Explosives – the Crystal Structure of ε-RDX as Determined by X-ray and Neutron Diffraction. *Chem. Commun.* **2010**, *46(31)*, 5662–5664.

[19] Dreger, Z. A.; Gupta, Y. M. Raman Spectroscopy of High-Pressure-High-Temperature Polymorph of Hexahydro-1,3,5-trinitro-1,3,5-triazine (ε-RDX). *J. Phys Chem A* **2010**, *114(26)*, 7038–7047.

[20] Dreger, Z. A.; Gupta, Y. M. Phase Diagram of Hexahydro-1,3,5-trinitro-1,3,5-triazine Crystals at High Pressures and Temperatures. *J. Phys Chem A* **2010**, *114(26)*, 8099–8105.

[21] Byrd, E. C. F.; Scuseria, G. E.; Chabalowski, C. F. An ab Initio Study of Solid Nitromethane, HMX, RDX, and CL20: Successes and Failures of DFT. *J. Phys. Chem. B* **2004**, *108(35)*, 13100–13106.

[22] Byrd, E. C. F.; Rice, B. M. Ab Initio Study of Compressed 1,3,5,7-Tetranitro-1,3,5,7-tetraazacyclooctane (HMX), Cyclotrimethylenetrinitramine (RDX), 2,4,6,8,10,12-Hexanitrohexaazaisowurzitane (CL-20), 2,4,6-Trinitro-1,3,5-benzenetriamine (TATB), and Pentaerythritol Tetranitrate (PETN). *J. Phys. Chem. C* **2007**, *111(6)*, 2787–2796.

[23] Miao, M. S.; Dreger, Z. A.; Winey, J. M.; Gupta, Y. M. Density Functional Theory Calculations of Pressure Effects on the Vibrational Structure of α-RDX. *J. Phys. Chem. A* **2008**, *112(47)*, 12228–12234.; Cui, H. L.; Ji, G. F.; Chen, X. R.; Zhu, W. H.; Zhao, F.; Wen, Y.; Wei, D. Q. First-Principles Study of High-Pressure Behavior of Solid β-HMX. *J. Phys. Chem. A* **2010**, *114(2)*, 1082–1092.; Zerilli, F. J.; Kuklja, M. M. Ab Initio Equation of State of the Organic Molecular Crystal: β-Octahydro-1,3,5,7-tetranitro-1,3,5,7-tetrazocine. *J. Phys. Chem. A* **2010**, *114(16)*, 5372–5376.

[24] Shimojo, F.; Wu, Z.; Nakano. A.; Kalia, R. K.; Vashisgta, P. Density Functional Study of 1,3,5-Trinitro-1,3,5-triazine Molecular Crystal with van der Waals Interactions. *J. Chem. Phys.* **2010**, *132(9)*, 094106-1–094106-8.

[25] Grimme, S. Semiempirical GGA-Type Density Functional Constructed with a Long-Range Dispersion Correction. *J. Comput. Chem.* **2006**, *27(15)*, 1787–1799.

[26] Sorescu, D. C.; Rice, B. M. Theoretical Predictions of Energetic Molecular Crystals at Ambient and Hydrostatic Compression Conditions Using Dispersion Corrections to Conventional Density Functionals (DFT-D). *J. Phys. Chem. C* **2010**, *114(14)*, 6734–6748.

[27] Balu, R.; Byrd, E. C. F.; Rice, B. M. Assessment of Dispersion Corrected Atom Centered Pseudopotentials: Application to Energetic Molecular Crystals. *J. Phys. Chem. B* **2011**, *115*, 803–810.

[28] Clark, S. J.; Segall, M. D.; Pickard, C. J.; Hasnip, P. J.; Probert, M. J.; Refson, K.; Payne, M. C. First Principles Methods Using CASTEP. *Z. Krystallogr.* **2005**, *220(5-6)*, 567–570.

[29] Perdew, J. P.; Burke, K.; Ernzerhof, M. Generalized Gradient Approximation Made Simple. *Phys. Rev. Lett.* **1996**, *77(18)*, 3865–3868.

[30] Vackar, J.; Hytha, M.; Simunek, A. All-Electron Pseudopotentials. *Phys. Rev. B* **1998**, *58(19)*, 12712–12720.

[31] Monkhorst, H. J.; Pack, J. D. Special Points for Brillouin-Zone Integrations. *Phys. Rev. B* **1976**, *13(12)*, 5188–5192.

[32] Fischer, T. H.; Almlof, J. General Methods for Geometry and Wave Function Optimization. *J. Phys. Chem.* **1992**, *96(24)*, 9768–9774.

[33] Gonze, X. First-Principles Responses of Solids to Atomic Displacements and Homogeneous Electric Fields: Implementation of a Conjugate-Gradient Algorithm. *Phys. Rev. B.* **1997**, *55(16)*, 10337–10354.

[34] Parker, S. F.; Carlile, C. J.; Pike, T. G.; Tomkinson, J.; Newport, R. J.; Andreani C. Ricci, F. P.; Sacchetti, F.; Zoppi, M. TOSCA: A World Class Inelastic Neutron Spectrometer. *Physica B* **1998**, *241-243*, 154–156.; Colognesi, D.; Celli, M.; Cilloco, F.; Newport, R. J.; Parker, S. F.; Rossi-Albertini, V.; Sacchetti, F.; Tomkinson, J.; Zoppi, M. TOSCA Neutron Spectrometer: The Final Configuration. *Applied Physics A - Materials Science & Processing* **2002,** *74(Suppl)*, S64–S66.

[35] Ramirez-Cuesta, A. J. aCLIMAX 4.0.1, The New Version of the Software for Analysing and Interpreting INS Spectra *Comput. Phys. Commun.* **2004**, *157*, 226–238.

[36] Tang, C. C.; Thompson, S. P.; Hill, T. P.; Wilkin, T. R.; Wagner, U. H. Design of Powder Diffraction Beamline (BL-I11) at Diamond. *Z. Kristallogr. Suppl.* **2007**, *26*, 153–158.

[37] Thompson, S. P.; Parker, J. E.; Potter, J.; Hill, T. P.; Birt, A.; Cobb, T. M.; Yuan, F.; Tang, C. C. Beamline I11 at Diamond: A New Instrument for High Resolution Powder Diffraction. *Rev. Sci. Instrum.* **2009**, *80*, 075107-1–075107-9.

[38] Mitchell, P. C. H.; Parker, S. F.; Ramirez-Cuesta, A. J.; Tomkinson, J *Vibrational Spectroscopy with Neutrons with applications in Chemistry, Materials Science and Catalysis*, World Scientific Publishing Co. Pte. Ltd., **2005**.

[39] Hagler, A.T.; Huler, E.; Lifson, S. Energy functions for peptides and proteins. I. Derivation of a Consistent Force Field Including the Hydrogen Bond from Amide Crystals. *J. Am. Chem. Soc.* **1974**, *96*, 5319–5327.

[40] Sandman, D. J.; Epstein, A. J.; Chickos, J. S.; Ketchum, J.; Fu, J. S.; Scheraga, H. A. Crystal Lattice and Polarization Energy of Tetrathiafulvalene. *J. Chem. Phys.* **1979**, *70*, 305–313.

[41] Pertsin, A. J.; Kitaigorodsky, A. I. *The atom-atom potential method applications to organic molecular solids*, Springer, Berlin, **1987**.

[42] Osborn, J. C.; York, P. A Comparison of Sublimation Enthalpies with Lattice Energies Calculated Using Force Fields. *J. Mol Struct.* **1999**, *474(1-3)*, 43–47.

[43] Bisker-Leib, V.; Doherty, M. F. Modeling the Crystal Shape of Polar Organic Materials: Prediction of Urea Crystals Grown from Polar and Nonpolar Solvents. *Cryst. Growth Des*. **2001**, *1(6)*, 455–461.

[44] Ouvrard, C. Mitchell, J. B. O. Can We Predict Lattice Energy from Molecular Structure? *Acta Cryst*. **2003**, *B59*, 676–685.

[45] Rogers, J. T. *Holston Defence Corporation, Kingsport, TN, Report HDC-20P-26-SER-B, CPIA Abstract 73-1016, AD 904-410L, U-B*, **1962**.

[46] Rosen, J.; Dickinson, C. Vapor Pressures and Heats of Sublimation of Some High-Melting Organic Explosives. *J. Chem. Eng. Data*, **1969**, *14*, 120–124.

[47] Perger, W. F.; Pandey, R.; Blanco, M. A.; Zhao, First-Principles Intermolecular Binding Energies in Organic Molecular Crystals. *Phys. Lett*. **2004**, *388*, 175–180.

[48] Hu, A.; Larade, B.; Dudiy, S.; Abou-Rachid, H.; Lussier, L.-S.; Guo, H. Theoretical Prediction of Heats of Sublimation of Energetic Materials Using Pseudo-Atomic Orbital Density Functional Theory Calculations. *Propell. Explos. Pyrotech.* **2007**, *32(4)*, 331–337.

[49] Wang, F.; Du, H.-C.; Zhang, J.-Y.; Gong, X.-D. Comparative Theoretical Studies of Energetic Azo s-Triazines. *J. Phys. Chem. A* **2011**, *115*, 11852–11860.

[50] Zhu, W.; Xiao, J.; Zhu, W.; Xia, H. Molecular Dynamics Simulations of RDX and RDX-Based Plastic-Bonded Explosives. *J. Hazard. Mat.* **2009**, *164(2-3)*, 1082–1088.

[51] Kitaigorodskii, A. I. *Molecular Crystals and Molecules*, Academic Press, New York and London, Vol. 29, **1973**.

[52] Chickos, J. S.; Braton, C. M.; Hesse, D. G.; Liebman, J. F. Estimating Entropies and Enthalpies of Fusion of Organic Compounds. *J. Org. Chem*. **1991**, *56(3)*, 927–938.

[53] Boese, R.; Downs, A. J.; Greene, T. M.; Hall, A. W.; Morrison, C. A.; Parsons, S. Polymorphism in the Crystal Structures of the Group 13 Trimethyls. *Organometallics* **2003***, 22(12)*, 2450–2457.

[54] Chadha, R.; Arora, P.; Saini, A.; Tain, D. S. An Insight into Thermodynamic Relationship Between Polymorphic Forms of Efavirenz. *J. Pharm. Pharmaceut. Sci*. **2012**, *15(2)*, 234–251.

[55] Fucke, K.; Quereshi, N.; Yufit, D. S.; Howard, J. A.K.; Steed, T. W. Hydrogen Bonding Is Not Everything: Extensive Polymorphism in a System with Conserved Hydrogen Bonded Synthons. *Cryst. Growth Des*. **2010**, *10(2)*, 880–886.

[56] Hall, P. G. Thermal Decomposition and Phase Transitions in Solid Nitramines. *Trans. Faraday Soc.* **1971**, *67*, 556–562.

[57] Kishore, K. Comparative Studies on the Decomposition Behaviour of Secondary Explosives RDX and HMX. *Def. Sci J.* **1978**, *28(2)*, 59–66.

[58] Zeman, S. Some Predictions in the Field of the Physical Thermal Stability of Nitramines. *Thermochim. Acta* **1997**, *302(1-2)*, 11–16.

[59] An extensive list inventory of methodologies used for crystal structure prediction can be found in the three blind tests carried out by the CCSD. (i) Lommerse, J. P. M.; Motherwell, W. D. S.; Ammon, H. L.; Dunitz, J. D.; Gavezzotti, A.; Hofmann, D. W.; Leusen, F. J.; Mooij, W. T. M.; Price, S. L.; Schweizer, B.; *et al*. A Teat of Crystal Structure Prediction of Small organic Molecules. *Acta Crystallogr., Sect. B: Struct. Sci.* **2000**, *56(4)*, 697–714. (ii) Motherwell, W. D. S.; Ammon, H. L.; Dunitz, J. D.; Dzyabchenko, A.; Erk, P.; Gavezzotti, A.; Hofmann, D. W. M.; Leusen, F. J. J.;

Lommerse, J. P. M.; *et al.* Crystal Structure Prediction of Small Organic Molecules: A Second Blind Test. *Acta Crystallogr., Sect. B: Struct. Sci.* **2002**, *58(4)*, 647–661. (iii) Day, G. M.; Motherwell, W. D. S.; Ammon, H. L.; Boerrigter, S. X. M.; Della Valle, R. G.; Venuti, E.; Dzyabchenko, A.; Dunitz, J. D.; Schweizer, B.; van Eijck, B. P.; *et al.* A Third Blind Test of Crystal Structure Prediction. *Acta Crystallogr., Sect. B: Struct. Sci.* **2005**, *61(5)*, 511–527.

[60] Oswald, I. D. H.; Millar, D. I. A.; Davidson, A. J.; Francis, D. J.; Marshall, W. G.; Pulham, C. R.; Cumming, A. S.; Lennie, A. R.; Warren, J. E. High-Pressure Structural Studies of Energetic Compounds. *High Pressure Res.* **2010**, *30(2)*, 280–291.

[61] Murnaghan, F. D. Finite Deformations of an Elastic Solid. *Am. J. Math.* **1937**, *59(2)*, 235–260.

[62] Miller, M. S. Thermophysical Properties of Cyclotrimethylenetrinitramine. *J. Thermophys. Heat Tansfer*, **1994**, *8(4)*, 803–805.

[63] Shoemaker, R. L.; Stark, J. A.; Taylor, R. E. Thermophysical Properties of Propellants. *High Temperatures High Pressures* **1985**, *17*, 429–435.

TOC Image

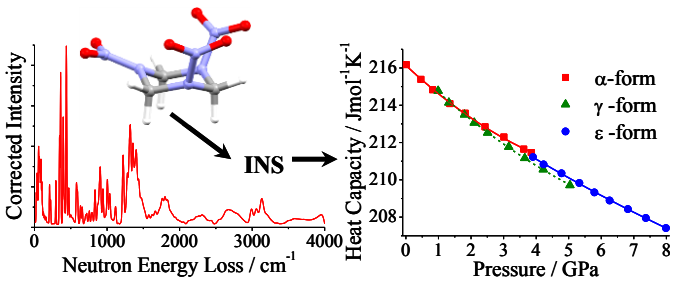

Prediction of heat capacities of α-, γ-, and ε-forms of RDX at high-pressures from complete vibrational information.